Supplementary Information

Activity and Durability of the Oxygen Reduction Reaction in a Nitrogen-Doped Rutile-Shell on TiN-Core Nanocatalysts Synthesised *via* Solution-Phase Combustion

Mitsuharu Chisaka,[a,*] *Yuta Ando*[a] *and Noriaki Itagaki*[a]

[a] Department of Electronics and Information Technology, Hirosaki University,

3 Bunkyo-cho, Hirosaki, Aomori 036-8561, Japan.

*Author to whom correspondence should be addressed.

Phone/Fax.: +81 172 39 3559, E-mail: chisaka@hirosaki-u.ac.jp (M. Chisaka)

S1. Surface crystal structure

Raman spectroscopy analyses were performed on some selected TiO_xN_y–C to investigate the surface crystal structures and oxygen defects in TiO_2. Figure S1 shows Raman spectra of TiO_xN_y–C with r = 100 after pyrolysis at two different T values 1123 K and 1273 K for 2 h under N_2 atmosphere. The typical Raman shifts for stoichiometric rutile-TiO_2 are ~142, ~446, and ~608 cm^{-1}, corresponding to the B_{1g}, E_g, and A_{1g} modes, respectively.[S1–S7] A broad peak at ~250 cm^{-1} was often observed for rutile TiO_2 and was assigned to either second-order scattering or dynamic disorder of TiO_6 octahedra.[S3] The Raman shifts for stoichiometric TiN are ~235, 320, 440, and 570 cm^{-1}, corresponding to transverse acoustic, longitudinal acoustic, second-order acoustic, and transverse optical modes, respectively.[S8, S9] Based on these assignments, the four peaks of the two TiO_xN_y–C shown in Fig. S1 are those of rutile TiO_2. Their XRD patterns showed different results; mixture of rutile TiO_2 and TiN observed at 1123 K was completely converted to a single TiN phase at 1273 K due to the enhanced reactivity between TiO_2 and urea or its by-products (Fig. 3). The different results observed from Raman spectroscopy against XRD should be originated from the lower depth in detection limit (the details are discussed in main body of the text) and the surface of TiN was oxidized to form rutile TiO_2. For the peak assigned to E_g mode in 1123 K sample, the Raman shift is lower than that of the stoichiometric rutile, ~446 cm^{-1} and it slightly shifted to lower positions further when T was increased to 1273 K, suggesting that oxygen defects were incorporated into the surface rutile TiO_2 of both samples and the amount of defects increased with increasing T.[S7,S10]

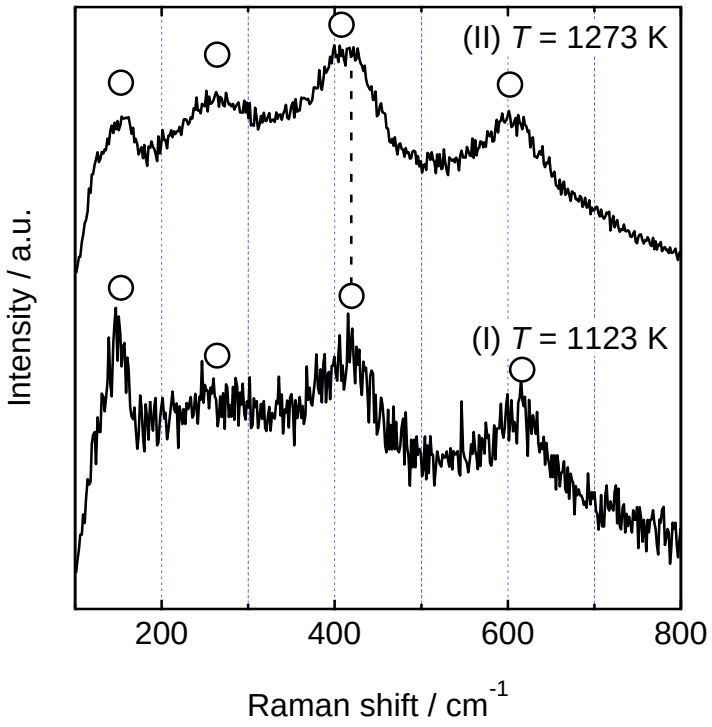

Figure S1. Raman spectra of TiO_xN_y–C with r = 100 after pyrolysis at different T of (I) 1123 K and (II) 1273 K for 2 h under N_2.

S2. Effect of *T* on ORR activity and selectivity of TiO_xN_y-C

Pyrolysis temperature under N_2 gas, *T*, was optimized for ORR activity and selectivity of TiO_xN_y–C with three different *r* values. Sets of RDE voltammograms and *n*–E_d curves of TiO_xN_y–C for *r* = 30 and 100 are shown in Fig. S2 and S3, respectively. In both samples, the optimum *T* was 1173 K, 50 K higher than that of *r* = 188 sample.[S11]

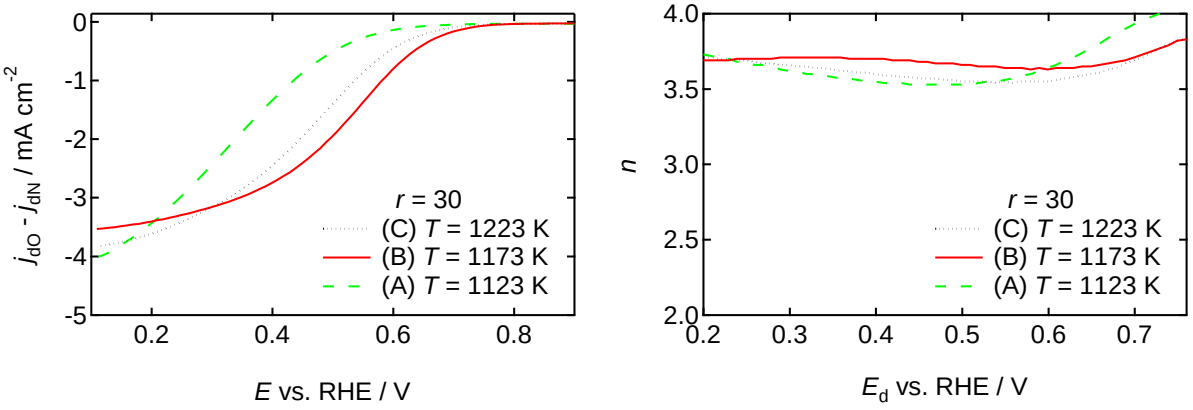

Figure S2. RDE voltammograms (left) and *n*–E_d curves (right) of TiO_xN_y–C for three different *T* of (A) 1123 K, (B) 1173 K and (C) 1223 K. The *r* was fixed at 30.

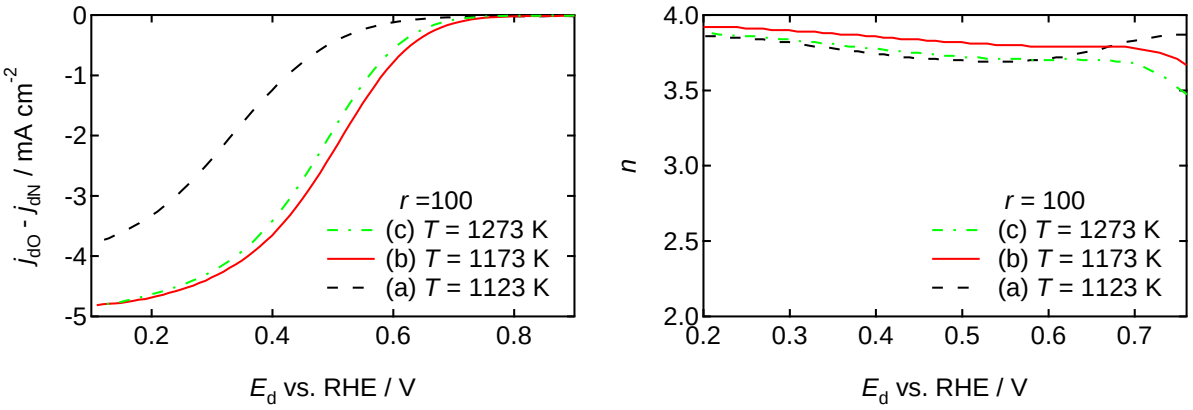

Figure S3. RDE voltammograms (left) and *n*–E_d curves (right) of TiO_xN_y–C for three different *T* of (a) 1123 K, (b) 1173 K and (c) 1273 K. The *r* was fixed at 100.

S3. Effect of *t* on crystal structure, chemical states and ORR activity of TiO_xN_y-C

The ORR activity was maximized by optimizing the *r* and *T* to 100 and 1173 K, respectively from Fig. 8 and S3. Effect of pyrolysis time, *t*, on some properties of TiO_xN_y–C was investigated at these conditions. Fig. S4, S5, S6 and S7 respectively shows XRD patterns, Ti 2p/N 1s spectra, s_z–*t* curves and RDE voltammograms of TiO_xN_y–C for three different *t* values. The nearly single TiN phase was observed when $t \leq 2$ h whereas rutile phase appeared at $t = 4$ h, indicating that TiN was oxidized when *t* was increased from 2 h to 4 h. It is suggested that all the nitrogen-source, i.e., urea and its by-products reacted with TiO_2 and therefore reductive atmosphere formed by the decomposition of nitrogen sources should be lost before *t* reached 4 h. Therefore, nitrogen atoms were lost at this high *T* of 1173 K. Their corresponding Ti 2p and N 1s spectra shown in Fig. S5 and the deconvolution results summarized in Fig. S6 agree well with these results; area fraction of Ti 2p peaks assigned to Ti–O–N/N–Ti–O bonding, s_2 decreased by 0.1 and N 1s peak became noisy when *t* was increased from 2 h to 4 h. The resulting activity of 4 h sample was lower than that of 2 h sample as shown in Fig. S7, suggesting that some of active defect sites on rutile TiO_2 created by nitrogen-doping were lost due to the removal of nitrogen atoms when *t* was increased from 2 h to 4 h.

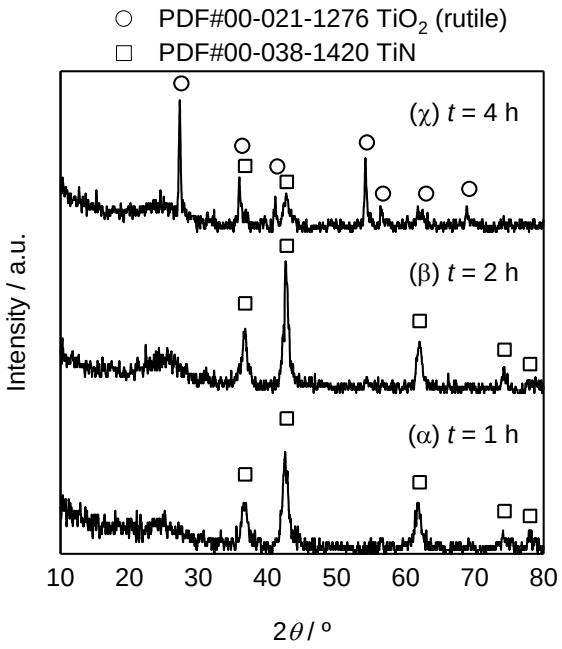

Figure S4. XRD patterns of TiO_xN_y–C after pyrolysis at T = 1173 K for three different t of (α) 1 h, (β) 2 h and (χ) 4 h. The r was fixed at 100.

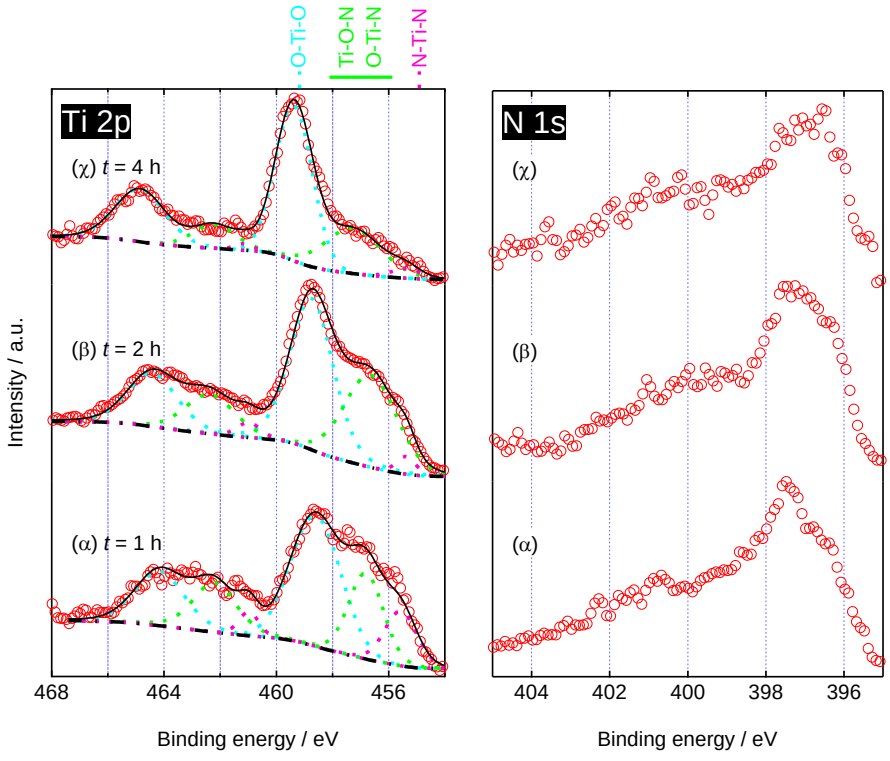

Figure S5. Ti 2p (left) and N 1s (right) spectra of TiO_xN_y–C after pyrolysis at T = 1173 K for three different t values; (α) 1 h, (β) 2 h and (χ) 4 h. The r was fixed at 100.

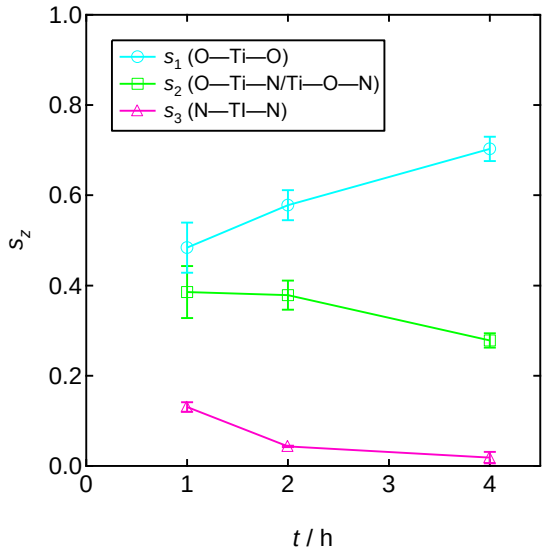

Figure S6. Area fractions of the three components shown in Fig. S5: s_1 (O–Ti–O bonding), s_2 (O–Ti–N/Ti–O–N bonding), and s_3 (N–Ti–N bonding).

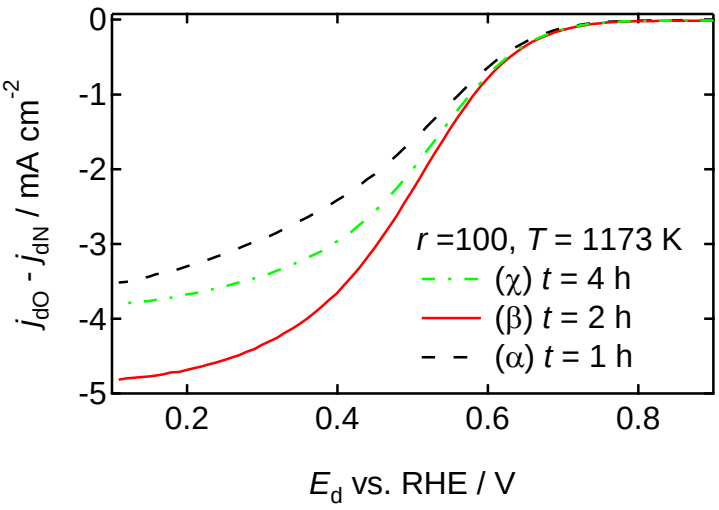

Figure S7. RDE voltammograms of TiO_xN_y–C after pyrolysis at T = 1173 K for three different t values; (α) 1 h, (β) 2 h and (χ) 4 h. The r was fixed at 100.

S4. The ORR mechanism on TiO_xN_y–C

RRDE voltammograms of TiO_xN_y–C that showed the highest activity were obtained with various rotation speed, ω, ranged from 400 rpm to 2500 rpm and are shown in Fig. S8. The disk current density after background correction, $|j_{dO} - j_{dN}|$ was independent on ω at $E_d > 0.7$ V, indicating that ORR proceeded under kinetic control. The diffusion limitation became dominant as E_d decreased, which is evidenced by the increase of $|j_{dO} - j_{dN}|$ with increasing ω. To further investigate the ORR mechanism, Koutecky-Levich plots obtained from Fig. S8 are shown in Fig. S9. The ORR mechanism was analysed using a following equation for a planar electrode covered with Nafion film[S12,S13]

$$J_d^{-1} = J_k^{-1} + J_l^{-1} + J_f^{-1} \qquad \text{(S1)}$$

where $J_d = -(J_{dO} - J_{dN})$, J_k, $J_l = B\omega^{1/2}$, and J_f are the background-corrected disk current, kinetically controlled current, O_2 diffusion limited current through the solution phase (B is the Levich constant), and O_2 diffusion-limited current through the Nafion film, respectively. In all the plots, J_d^{-1} is linear with respect to $\omega^{-1/2}$ and they are essentially parallel. The value of the intercept is expressed as $J_k^{-1} + J_f^{-1}$ because the term J_l^{-1} should be zero at $\omega \to \infty$. The intercept decreased with decreasing E_d and it became negligible at $E_d \leq 0.4$ V, indicating that both J_k^{-1} and J_f^{-1} are small and thus ORR proceeded under solution phase O_2-diffusion limited control at the E_d region. The Nafion film resistance, J_f^{-1} should be independent of E_d. Therefore, the values of J_f^{-1} at any E_d were assumed negligible to obtain J_k.

Accelerated degradation tests were performed using the best catalyst and Figure S10 shows the RDE voltammograms before and after 20,000 potential cycles in O_2 atmosphere. Their J_k values were calculated as described above and resulting Tafel plots are shown in Fig. 10.

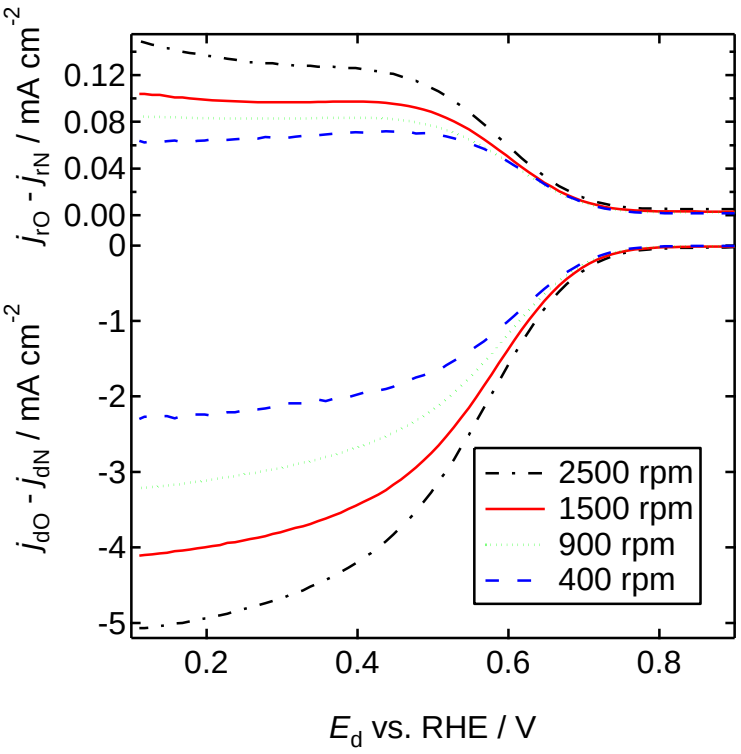

Figure S8 RRDE voltammograms of TiO_xN_y–C for four ω, 400, 900, 1500 and 2500 rpm. The r, T and t were fixed at the optimum values of 100, 1173 K and 2 h, respectively.

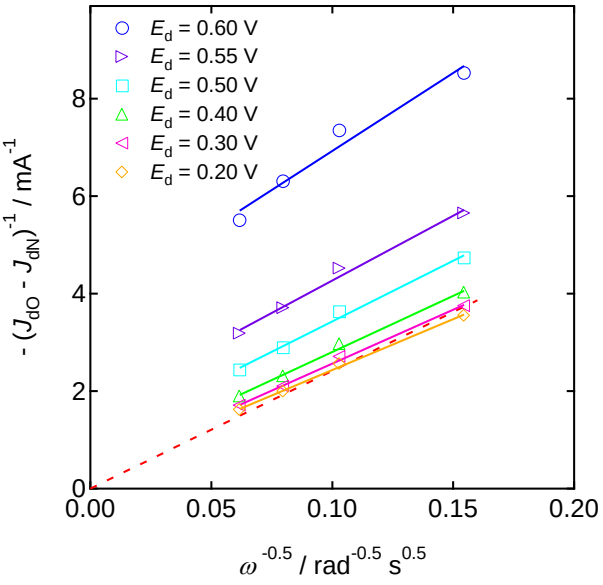

Figure S9 Koutecky-Levich plots of TiO_xN_y–C obtained from Fig. S8 (Markers and solid lines) and an ideal planar electrode that catalyse ORR completely *via* a 4-electron reaction pathway without Nafion film calculated using a so-called Levich equation (dashed line).

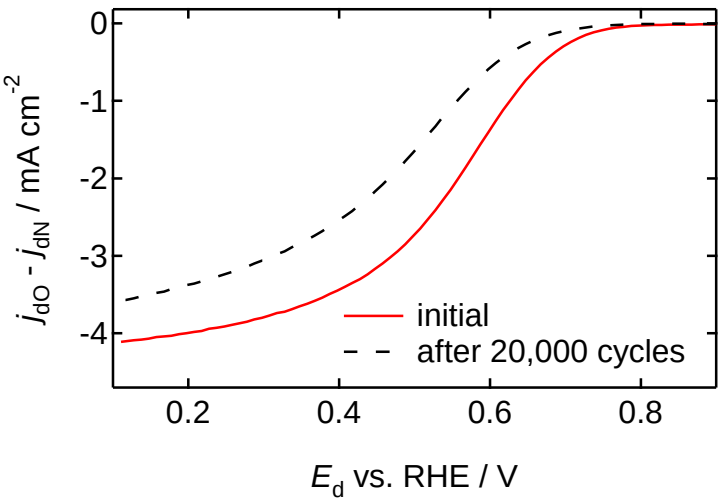

Figure S10 RDE voltammograms of TiO_xN_y–C (r = 100, T = 1173 K) before and after 20,000 potential cycles. Cycling was performed between 0.6 and 1.0 V vs. RHE at a scan rate of 50 mV s^{-1} in O_2-saturated 0.1-mol dm^{-3} H_2SO_4.

S5. Active site for ORR on TiO_xN_y-C

To investigate the active site for ORR on TiO_xN_y–C, ZrO_xN_y–C catalysts were synthesized by using ZrF_4 (Sigma-Aldrich Co., St. Louis, Missouri, U.S.) instead of TiF_4. All the other experimental conditions used for ZrO_xN_y–C were identical to those for TiO_xN_y–C that showed the highest activity; the synthesis conditions were r = 100, T = 1173 K and t = 2 h. The RDE voltammograms of TiO_xN_y–C and ZrO_xN_y–C are shown in Fig. S11. The TiO_xN_y–C showed higher $|j_{dO} - j_{dN}|$ than ZrO_xN_y–C at any E_d, indicating that the oxynitride particles determined the activity of these catalysts. If the activity of these two catalysts were originated from nitrogen-doped carbon species, these two voltammograms should be identical because all the following parameters were identical; the content of carbon supports, urea and pyrolysis conditions. Therefore, these results indicate that the activity of TiO_xN_y–C was, at least at high E_d, originated from TiO_xN_y, not from nitrogen-doped carbon species.

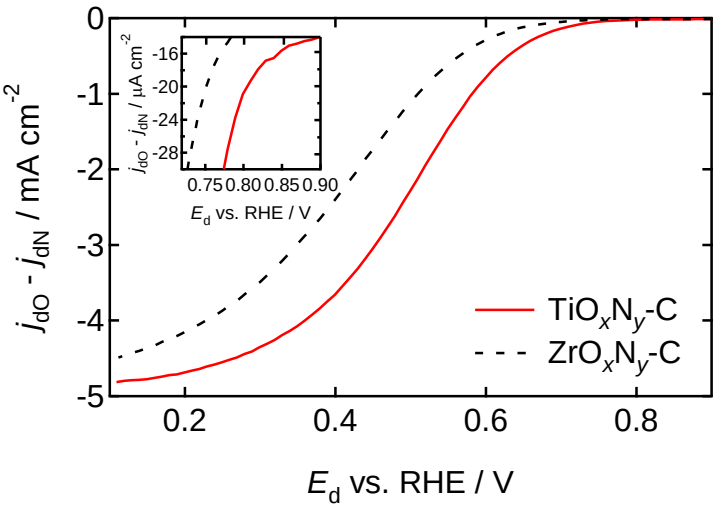

Figure S11. RDE voltammograms of TiO_xN_y–C and ZrO_xN_y–C after pyrolysis at T = 1173 K for 2 h under N_2 atmosphere. The r was fixed at 100.

References

(S1) S. P. S. Porto, P. A. Fleury and T. C. Damen, *Phys. Rev.*, 1967, **154**, 522.

(S2) R. J. Capwell, F. Spagnolo and M. A. DeSesa, *Appl. Spectrosc.*, 1972, **26**, 537.

(S3) U. Balachandran and N. G. Eror, *J. Solid State Chem.*, 1982, **42**, 276.

(S4) R. J. Betsch, H. L. Park and W. B. White, *Mat. Res. Bull.*, 1991, **26**, 613.

(S5) H. Cheng, J. Ma, Z. Zhao and L. Qi, *Chem. Mater.*, 1995, **7**, 663.

(S6) S. M. Oh, J. G. Li and T. Ishigaki, *J. Mater. Res.*, 20 (2005) 529

(S7) X. H. Wang, J. G. Li, H. Kamiyama, M. Katada, N. Ohashi, Y. Moriyoshi and T. Ishigaki, *J. Am. Chem. Soc.*, 2005, **127**, 10982.

(S8) Y. H. Cheng, B. K. Tay, S. P. Lau, H. Kupfer and F. Richter, *J. Appl. Phys.*, 2002, **92**, 1845.

(S9) W. Spengler, R. Kaiser, A. N. Christensen and G. Müller-Vogt, *Phys. Rev. B*, 1978, **17**, 1095.

(S10) M. Chisaka, A. Ishihara, K. Suito, K. Ota and H. Muramoto, *Electrochim. Acta*, 2013, **88**, 697.

(S11) M. Chisaka, Y. Ando and H. Muramoto, *Electrochim. Acta*, 2015, **183**, 100.

(S12) U. A. Paulus, T. J. Schmidt, H. A. Gasteiger and R. J. Behm, *J. Electroanal. Chem.*, 2001, **495**, 134.

(S13) E. Higuchi, H. Uchida and M. Watanabe, *J. Electroanal. Chem.*, 2005, **583**, 69.